



Modeling and simulation of the intermittent swimming gait with the muscle-contraction model of pre-strains

Zhijie Zhao, Lei Dou*

National Key Laboratory of Transient Physics, Nanjing University of Science and Technology, Nanjing, China

ARTICLE INFO

Keywords:

Intermittent swimming
Active distortions
Energy saving
Biomechanics
Fluid-structure interaction

ABSTRACT

The muscle-contraction model of pre-strains is employed to study the intermittent swimming gait of a 2D freely swimming fish. The fluid-structure interaction problem of fish swimming is solved with the finite elements method. Benefits of the intermittent swimming and the effects of the duty cycle and the tail swing number in a burst phase are emphasized. The results show that, compared to the steady swimming, a huge energy saving for swimming can be achieved by sacrificing a little speed during the intermittent swimming. Moreover, the fish swimming can be gradually transited from an intermittent mode to the continuous mode by increasing the duty cycle. With a smaller duty cycle, the fish can save more energy to obtain the same swimming velocity. A smaller tail swing number in a burst phase is more helpful to improve the energy utilization rate under the condition of $R_{duty} = 0.5$. In addition, the intermittent swimming will have more benefits at the lower and the higher average swimming speeds, and it is very important to have a proper proportion of the velocity bounds for the performance improvement of the intermittent swimming. These conclusions may have direct meanings for the development of biomimetic autonomous underwater vehicles.

1. Introduction

Many flying and swimming animals exhibit an intermittent locomotion behavior compared to the continuous locomotion. In the aquatic environment, the burst-and-coast swimming is widely used by fishes and marine mammals, such as salmons, tetras and seals (Calovi et al., 2017; Williams, 2001). In addition, birds use the interspersed periods of flapping and gliding, known as the undulating flight mode (Rayner et al., 2001; Ribak et al., 2005; Tobalske, 2001; Tobalske et al., 2010). The diversity and convergence are coexisting in the locomotion strategies of animals. Scaradozzi et al. (2017) reviewed the classification of fish locomotion modes and the biological propulsion principles for the development of biomimetic autonomous underwater vehicles (AUVs). The strategy of intermittent locomotion was regarded as a result of the convergent evolution under the great pressure for efficient locomotion (Gleisset al., 2011). Specifically, the intermittent locomotion consists of the active burst flying or swimming and the inactive gliding, in which the body is kept straight and motionless (Videler and Weihs, 1982).

In the past decades, researchers have been intrigued by the intermittent locomotion behavior of animals, especially the burst-and-coast swimming. Theoretically, an analysis of the mechanics of burst-and-

coast swimming showed a large energy saving of more than 50% compared with the steady swimming (Weihs, 1974). Wu et al. (2007) examined the body kinematics and the flow in the wakes of koi carps swimming in a burst-and-coast mode by experiment. An energy saving of about 45% was estimated for the burst-and-coast swimming of the koi carps compared with the steady swimming at the same mean speed. A comparative study on the flow fields of fish larvae and adults in the burst-and-coast swimming was conducted by Müller et al. (2000). Mwaffo et al. (2017) studied the burst and cruise swimming movements of zebrafish using particle image velocimetry. Obviously, it is difficult to conduct experiments directly on live fishes due to the complexity and uncontrollability of the fish behaviors. Experimental and numerical simulation methods of bio-inspired robots have been widely applied to study the mechanics principles underlying biological swimming (Costa et al., 2019, 2018, 2017; Chan et al., 2007). Floryan et al. (2017) studied the intermittent swimming motions of a rigid pitching foil in a recirculating free-surface water channel. In general, the intermittent locomotion is often accompanied by the changes in depth for marine animals. These species show an undulating flight behavior like birds by using their negative buoyancy. The fish sink down into the deeper water by gliding and then actively swim upwards to the original depth (Gleiss

* Corresponding author.

E-mail addresses: zhaozhijiefm@163.com (Z. Zhao), douleijs@163.com (L. Dou).

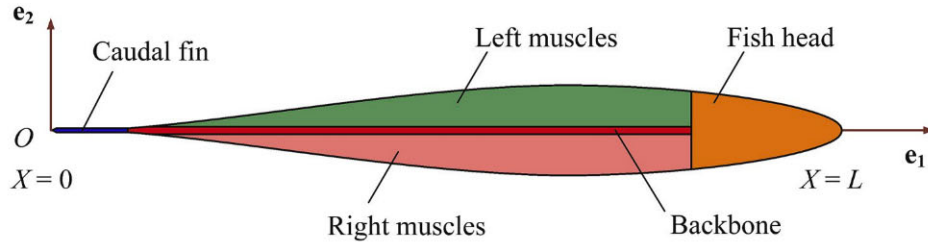


Fig. 1. Schematic of the 2D fish model.

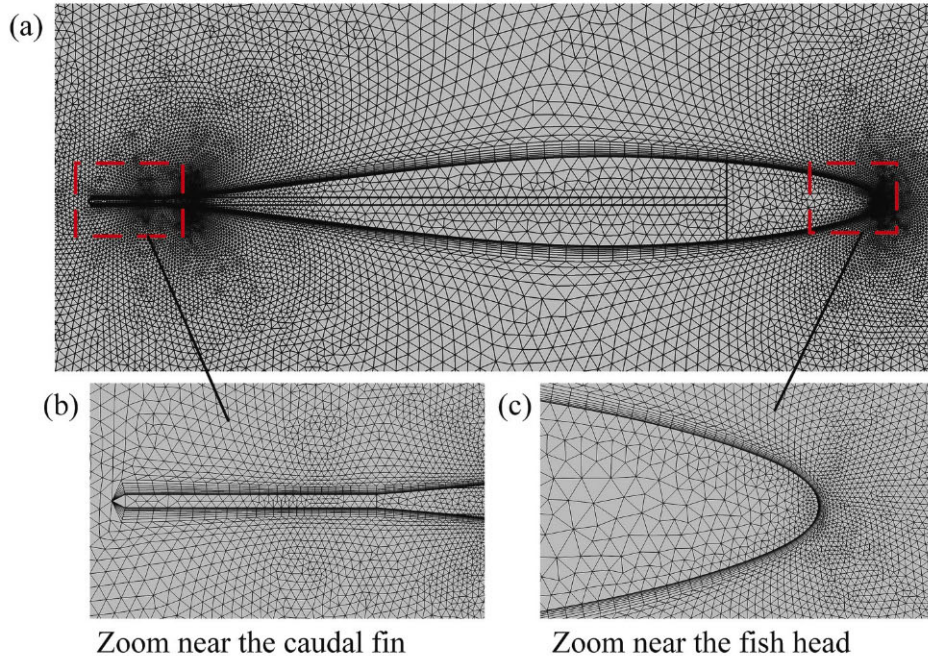


Fig. 2. Mesh details of the 2D fish model.

et al., 2011). A transformation of the potential energy into kinetic energy is made during the gliding, which is considered to provide a saving of mechanical power. On the other hand, many fish species who are neutrally buoyant still tend to adopt an intermittent locomotion style (Iosilevskii, 2016; Weihs, 1974). This indicates that the intermittent locomotion is generally used by swimming animals and is bound to have significant advantages compared to the continuous locomotion. However, up to now, most of existing studies are focused on the continuous locomotion style, especially in the aspect of numerical simulation. Numerical studies are helpful to shed lights on the mechanisms of fish steady swimming (Borazjani and Sotiropoulos, 2008; Chang et al., 2012; Xia et al., 2015; Zhang et al., 2018; Zhu et al., 2002). In contrast, numerical studies of the intermittent locomotion are relatively few (Akoz and Moore, 2017; Takagi et al., 2013; Xia et al., 2018).

In this paper, we consider a neutrally buoyant fish that performs a burst-and-coast swimming at a constant depth, and thus a 2D numerical study is feasible. The fish swimming was widely studied by the 2D numerical simulations (Bao et al., 2017; Xu et al., 2017; Deng et al., 2006; Karbasian; Esfahani, 2017; Sun et al., 2018; Xiao and Liao, 2010; Zhang and Zheng, 2009). Essentially, the mechanical power needed by a swimming fish is generated by the muscles (Rome et al., 1993) and the process of swimming is a typical problem of fluid-structure interaction (FSI). Therefore, a proper modeling of the muscle contraction and an effective solving scheme of the FSI problem are vital to the simulation of fish swimming. For the past few years, the notion of active distortions, also known as the pre-strains, has been successfully applied to model the muscle functioning (Evangelista et al., 2011; Nardinocchi et al., 2013;

Nardinocchi et al., 2013, 2007; Shaw et al., 2015). Curatolo and Teresi (2016) creatively adopted the muscle-contraction model of pre-strains to study the steady swimming of a virtual carangiform fish. Following Curatolo and Teresi (2016), we will model the intermittent swimming gait of a carangiform fish with the muscle-contraction model of pre-strains.

The remaining of the paper is organized as follows. In Section 2, the details of the fish model and the adopted simulation method will be introduced. In Section 3, a comparative study on the intermittent swimming gait of the virtual fish with the continuous swimming mode will be performed. Then, the effects of the duty cycle and the tail swing number in a burst phase on the propulsive performance will be investigated. In addition, the results of present study will be compared with the previous researches. Finally, we will summarize the conclusions of this work and will outline the future research directions in Section 4.

2. Material and methods

As previously mentioned, a neutrally buoyant fish swimming at a constant depth is considered. In view of the absence of up-and-down motion, a 2D simplification is possible to grasp the key features of fish swimming. The FSI problem of swimming is solved with the finite elements method (FEM) by using the commercial software of COMSOL Multiphysics (version 5.4). The surrounding fluid of the fish is set as the liquid water modeled with the Navier-Stokes equations. The fish body is modeled as an isotropic and linear elastic material, whose bending motion is stimulated by a time-varying field of pre-strains.

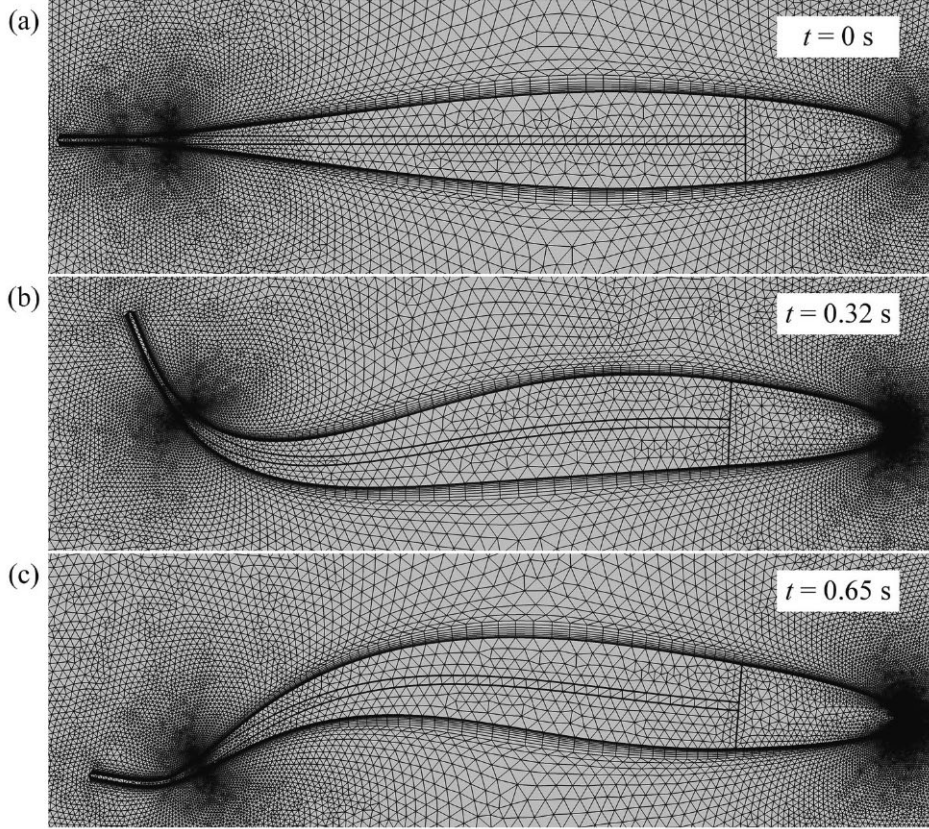


Fig. 3. Moving mesh and automatic re-meshing. The changes of computational grids near the fish model with time.

2.1. Fish model

As shown in Fig. 1, a 2D streamlined fish model is mainly made up of a NACA 64012 foil, whose chord length is $c = 0.1$ m. The trailing edge of the foil is truncated at the 95% chord length point. Then, a caudal fin with a uniform width of about $0.0051c$ is attached to the caudal peduncle. The length of the caudal fin is $0.1c$ and a chamfering is made at the tip of caudal fin. Ultimately, this bilaterally symmetrical fish model has a total length of $L = 0.105$ m. Apart from the caudal fin, the rest part of the fish model is divided into four parts. With a relatively inflexible anterior body section, the fish head is modeled as a rigid domain with an axial length of $0.2c$. The muscles of the fish body are divided into the right and the left halves by the backbone in the middle portion of the fish body. We do not perform a functional segmentation of the fish muscles, in spite of that the muscles may have two principal types: the slow-twitch or red muscles, and the fast-twitch or white muscles (Altringham and Ellerby, 2000; Jayne and Lauder, 1994; Rome et al., 1988). Different muscle types may have different mechanical and energetic properties, and this issue is beyond the scope of this study. The backbone has a uniform width of $0.001c$. In this fish model, only the right and left muscles are actively stimulated to produce the contraction and relaxation. That means the movements and deformations of the backbone and the caudal fin are entirely passive. Although previous studies have shown that the fins of fish are actively controlled by the musculoskeletal or musculo-vascular systems (Flammang and Lauder, 2009; Pavlov et al., 2017; Ren et al., 2016). As shown in Fig. 1, the fish model is defined in a Cartesian coordinate system ($O: e_1, e_2$), with the origin O at the tip of caudal fin, and e_1 passes through the axis of symmetry of the fish model. Two coordinate variables of X and Y are corresponding to the coordinate axes e_1 and e_2 , therefore, the tip of caudal fin and the tip of nose can be represented as $(0, 0)$ and $(L, 0)$, respectively. Fig. 2 gives the mesh details of the fish model used in this paper. Triangular meshes are generated in both the fluid domain and the

solid domain, and finer quadrilateral meshes are adopted near the fluid-solid boundary between the fish model and the surrounding fluid.

2.2. Numerical method

The swimming of the fish is simulated by using the FSI interface of COMSOL Multiphysics. The interface models both the fluid domain and the solid domain and includes a predefined condition for the interactions at the fluid-solid boundary. Using a time-dependent study, the FSI interface considers the two-way coupling effects between the deformable solid (fish model) and the surrounding fluid (liquid water). In order to track the path of long-distance swimming, both moving mesh and automatic re-meshing technologies are applied. Fig. 3 shows the change of meshes during the swimming, indicating a successful simulation of the undulation movement of fish.

Usually, the lateral undulating motion of the fish midline is assigned as a backward traveling wave in the fish swimming simulations (Gao and Triantafyllou, 2018; Li et al., 2017; Sun et al., 2018). In fact, however, what we observed in the swimming of a live fish is a result of the interactions between the muscle actions and the water resistances. Therefore, the FSI effects are vital for the simulation of fish swimming. Following Curatolo and Teresi (2016), we model the muscle contraction and relaxation through the notion of active distortions (pre-strains) and simulate the fish swimming by solving the two-way FSI problem. In contrast, we put emphasis on the intermittent swimming gait instead of the steady swimming. Firstly, we make the fish muscles contract and relax alternately by applying the time-varying pre-strains. Then, forces will arise in the muscles when the motion is hampered by the surrounding water, resulting in the desired fish swimming movement.

The computational domain Ω consists of a solid domain (fish model) Ω_s and a fluid domain (liquid water) Ω_f . The interface between the solid domain and the fluid domain (the FSI boundary) is represented as $\partial\Omega_{st}$. State variables of the problem include: the solid displacement field $\mathbf{u} =$

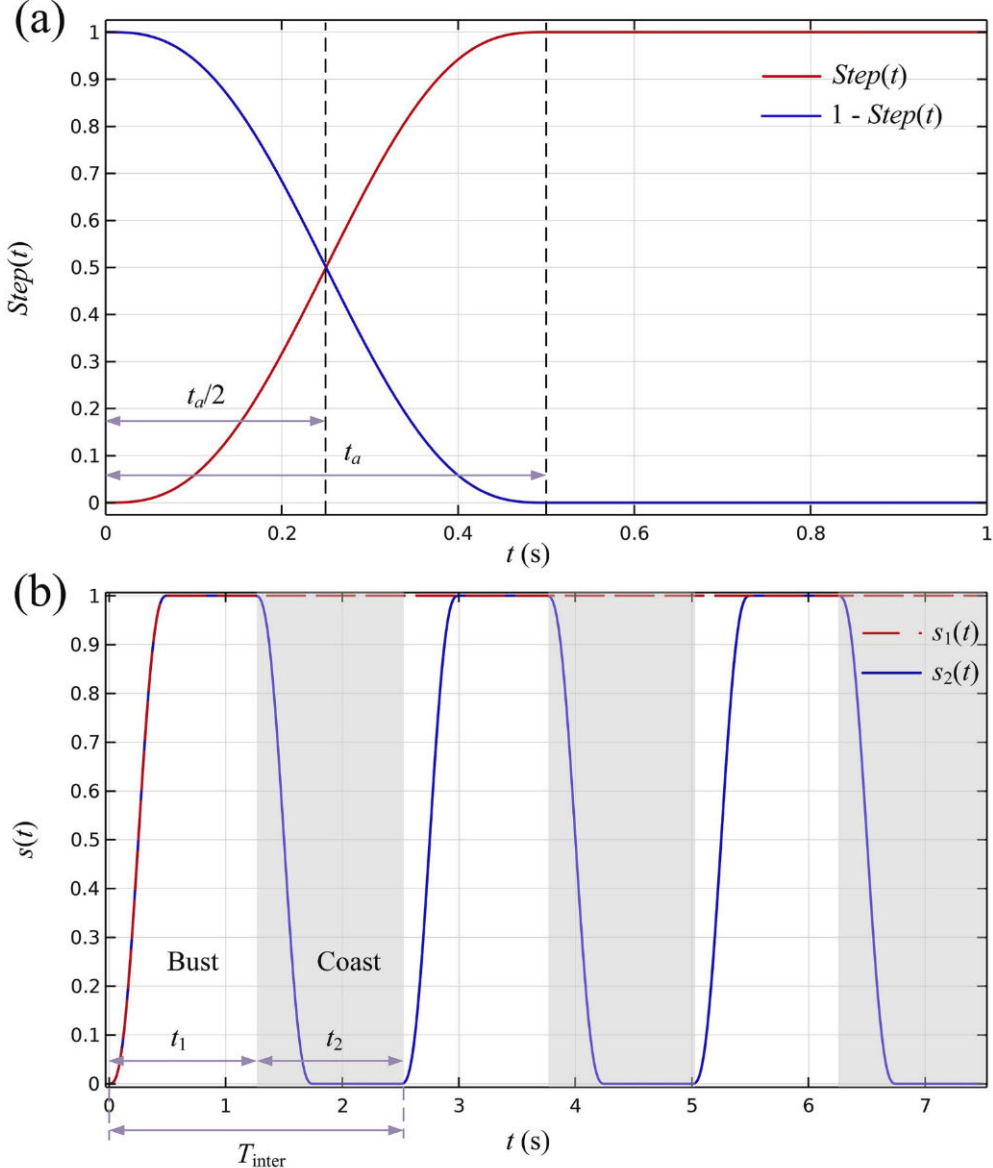


Fig. 4. (a) Graphs of the step functions $Step(t)$ and $1 - Step(t)$. (b) Comparison of the time functions of $s_1(t)$ and $s_2(t)$, corresponding to the steady swimming and the intermittent swimming, respectively.

Table 1
Key parameters of the simulation model.

Fluid		
ρ_f	1000 kg/m ³	Fluid mass density
μ	0.001 Pa·s	Fluid dynamic viscosity
Fish model		
ρ_s	1050 kg/m ³	Fish mass density
ν	0.3	Poisson modulus
Y_m	0.7 MPa	Fish muscles Young's modulus
Y_f	0.2 MPa	Fish fin Young's modulus
Y_b	0.2 MPa	Fish backbone Young's modulus
Kinematics		
L	0.105 m	Fish total length
L_b	0.2132 m	Fish contour length
ε_{\max}	0.12	The maximum contraction amplitude of muscles
T	$1/f$	Fish tail beat period
T_{inter}	nT	The time period of the intermittent swimming
t_a	0.5 s	Transition time

Table 2
Characteristics of three different meshes for grid sensitivity investigations.

Mesh name	Number of points on the FSI boundaries	Number of cells
mesh a	225	3.61×10^4
mesh b	331	7.48×10^4
mesh c	557	1.02×10^5

(u_1, u_2) , describing the displacement of the fish model, the fluid velocity field $\mathbf{v} = (v_1, v_2)$, representing the velocity distribution of the surrounding water. The equations describing the fluid domain are the Navier-Stokes equation for conservation of momentum and the continuity equation for conservation of mass:

$$\rho_f \frac{\partial \mathbf{v}}{\partial t} + \rho_f (\mathbf{v} \cdot \nabla) \mathbf{v} = \nabla \cdot [-p \mathbf{I} + \mathbf{K}] + \mathbf{f}, \quad (1)$$

$$\rho_f \nabla \cdot (\mathbf{v}) = 0. \quad (2)$$

The equation describing the balance of forces on the solid domain

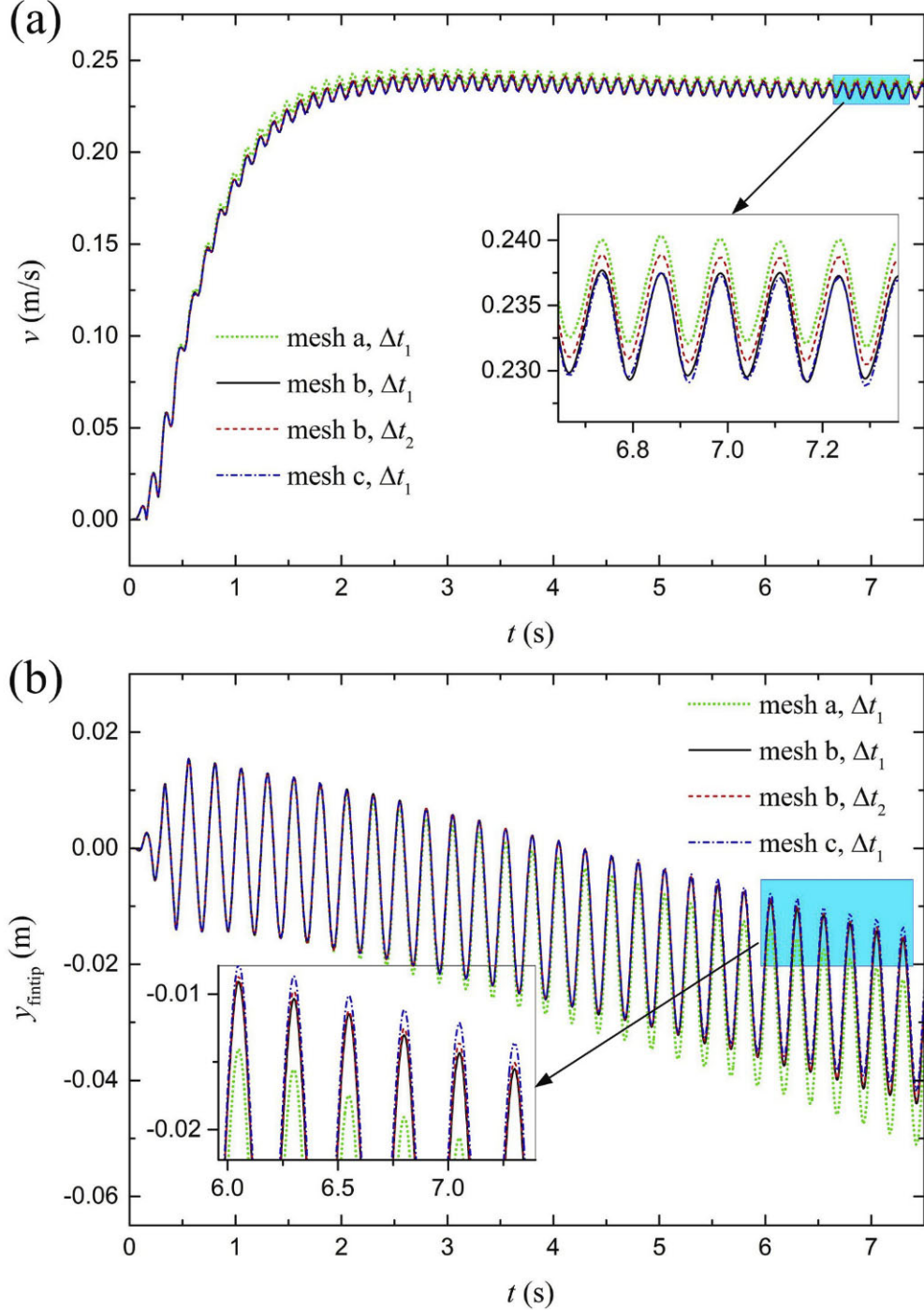


Fig. 5. The time histories with different meshes and temporal resolution for the steady swimming case with $f = 4$ Hz, $\lambda = L$, $n = 10$ and $R_{duty} = 0.5$. (a) The transient swimming velocity of the fish (v). (b) The Y coordinate of the caudal fin tip (y_{fintip}).

can be expressed as:

$$\rho_s \frac{\partial^2 \mathbf{u}}{\partial t^2} = \nabla \cdot \mathbf{S} + \mathbf{f}_v. \quad (3)$$

In these equations, ρ_f and ρ_s are the mass density of the fluid and the solid, respectively. p is the pressure of the fluid and \mathbf{I} denotes the unit diagonal matrix. \mathbf{f} is the external forces applied to the fluid and \mathbf{f}_v is the volumetric force exerted on the solid. Moreover, the fluid is assumed to be incompressible ($\rho_f = \text{constant}$). The stress of the fluid is $\boldsymbol{\Gamma} = -p\mathbf{I} + \mathbf{K}$, where $\mathbf{K} = \mu[\nabla \mathbf{v} + (\nabla \mathbf{v})^T]$ represents the viscous part of the fluid stress. Here, μ is the dynamic viscosity of the fluid. The deformation

gradient of the solid is $\mathbf{F} = \mathbf{I} + \nabla \mathbf{u}$ and a multiplicative decomposition of $\mathbf{F} = \mathbf{F}_e \mathbf{F}_0$ is made. Here, \mathbf{F}_e and \mathbf{F}_0 are the elastic deformation and a time-varying distortions field, respectively. Correspondingly, the non-linear strain measures are defined as:

$$\mathbf{E} = \frac{1}{2}(\mathbf{F}^T \mathbf{F} - \mathbf{I}), \quad \mathbf{E}_0 = \frac{1}{2}(\mathbf{F}_0^T \mathbf{F}_0 - \mathbf{I}), \quad (4)$$

where the superscript ' T ' denotes the matrix transpose. Consequently, the elastic strain can be represented as $\mathbf{E}_e = \mathbf{E} - \mathbf{E}_0$. The reference stress of the solid is given by:

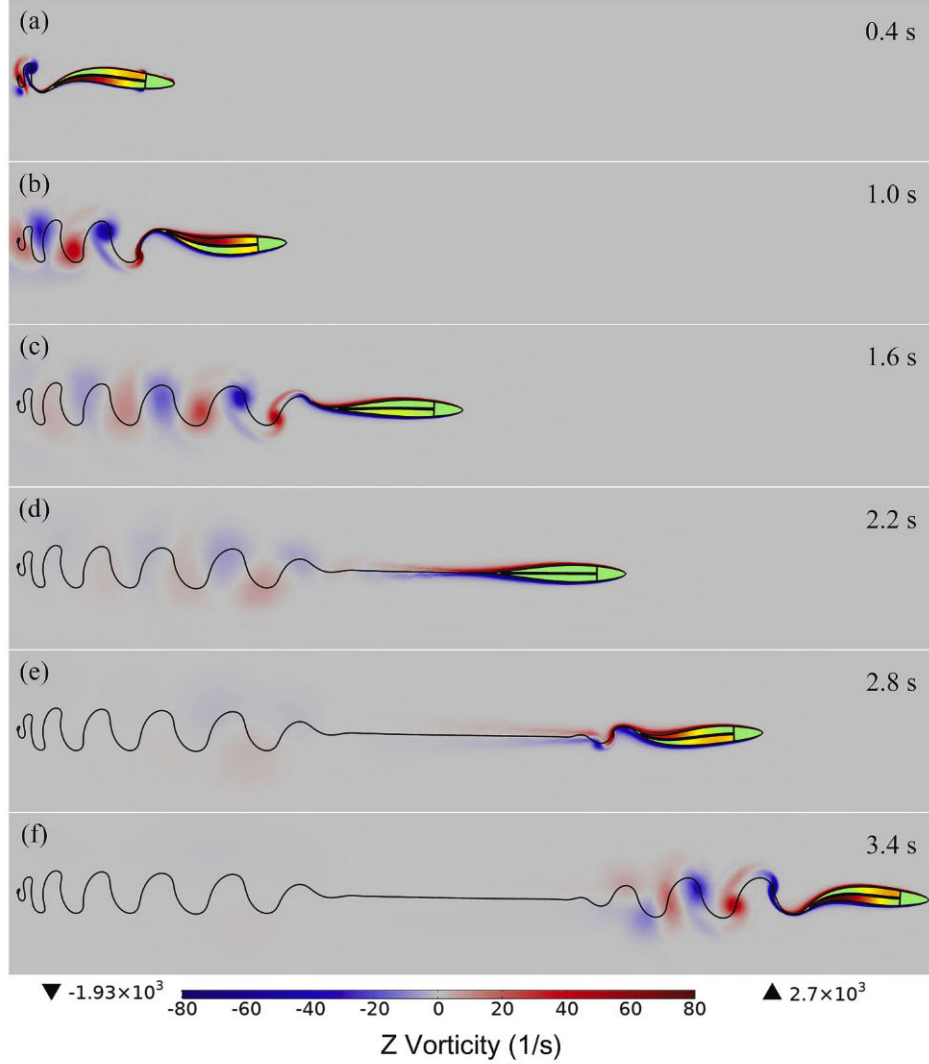


Fig. 6. Snapshots of a burst-and-coast swimming case with $f = 4$ Hz, $\lambda = L$, $T_{\text{inter}} = 10T$, and $R_{\text{duty}} = 0.5$. The vorticity field is depicted and the motion trajectory of the caudal fin tip is also plotted with a black solid line. The related animations of the burst-and-coast swimming simulation and the relevant steady swimming simulation are provided in the supplementary movies as [Movie S1](#) and [Movie S2](#), respectively.

$$\mathbf{S} = \mathbf{F}_c \mathbf{S}_e \mathbf{F}_0^*$$

(5)

$$\mathbf{S}_e = \frac{Y}{(1+\nu)} \mathbf{E}_e + \frac{\nu Y}{(1+\nu)(1-2\nu)} \text{tr}(\mathbf{E}_e) \mathbf{I}, \quad (6)$$

where Y and ν are the Young's modulus and the Poisson modulus of the solid, respectively, and $\mathbf{F}_0 = \text{Det}(\mathbf{F}_0)(\mathbf{F}_0^{-1})^T$. As mentioned above, the muscles function is modeled by the active distortions (pre-strains) of $\mathbf{E}_0 = \mathbf{E}_0(X, Y, t)$. In addition, the system of Eqs. (1)–(3) is subject to the FSI boundary conditions:

$$\mathbf{T}\mathbf{n} = -(-p\mathbf{I} + \mathbf{K})\mathbf{n}, \quad \mathbf{v} = \dot{\mathbf{u}}, \quad (7)$$

where $\mathbf{T} = \mathbf{S}(\mathbf{F}^*)^{-1}$ denotes the actual stress in the solid and \mathbf{n} is the outward unit normal vector to the boundary. The force exerted on the boundary of the fish body is the fluid reaction force induced by the movements of fish. Moreover, the fluid velocity on the FSI boundary equals to the movement speed of the fish body. It should be noted that the computational domain is a rectangular virtual aquarium with a length of 6 m and a width of 1 m. All the four boundaries of the aquarium are set as no-slip walls. For more details about the simulation method, see the literature ([Curatolo and Teresi, 2016](#)) and the help files of COMSOL Multiphysics ([COMSOL Inc, 2018](#)).

2.3. Swimming modes

As mentioned above, the research of burst-and-coast swimming mode is the emphasis in this paper. For comparing, the steady swimming mode is also considered. In order to imitate the swimming of a carangiform fish, the muscular movements are modeled by the time-varying distortions with the following forms ([Curatolo and Teresi, 2016](#)):

$$E_0^l(X, Y, t) = -\epsilon_{\max} \sin\left(\frac{\omega t + \gamma X}{2}\right)^2 h(X)s(t), \quad (8)$$

$$E_0^r(X, Y, t) = -\epsilon_{\max} \sin\left(\frac{\omega t + \gamma X + \pi}{2}\right)^2 h(X)s(t). \quad (9)$$

The superscripts '*l*' and '*r*' denote the left halve and the right halve of the fish muscles, respectively. Based on this model, the fish swims with an angular frequency of $\omega = 2\pi f$ and a wave number of $\gamma = 2\pi/\lambda$, here, f and λ represent the tail beat frequency and the wavelength of the fish undulation, respectively. The parameter ϵ_{\max} is the maximum contraction amplitude of the fish muscles.

$$h(X) = \frac{(X^2 - L^2)}{L^2}, \quad (10)$$

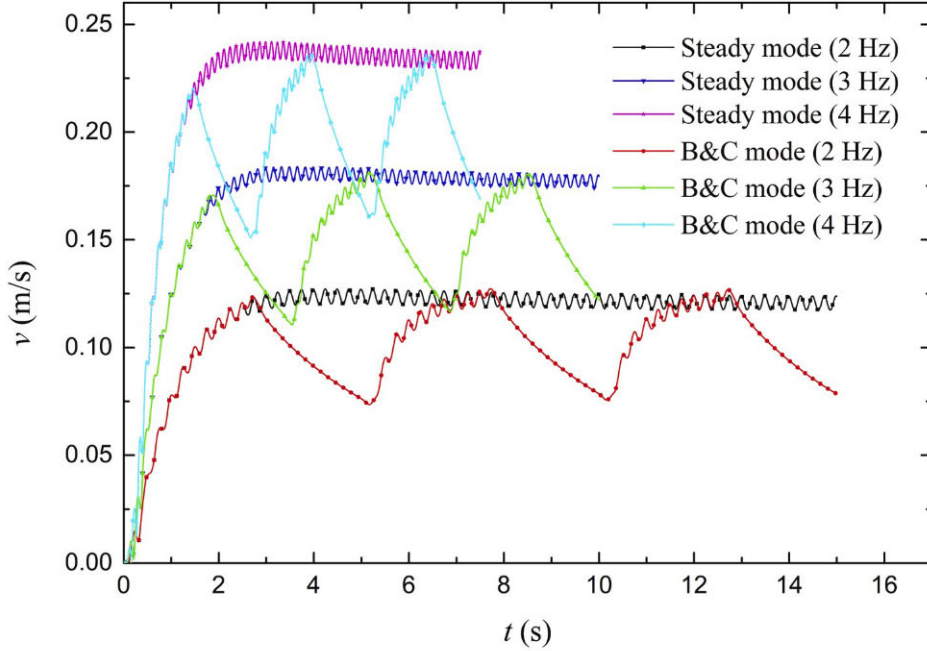


Fig. 7. Time histories of the swimming velocity of the intermittent swimming (B&C mode) and the relevant steady swimming (steady mode). For clarity, the figure shows only the data of the integer frequency cases.

$$s_1(t) = \text{Step}(t), \quad (11)$$

$$s_2(t) = \text{Step}(t) \cdot (t < R_{\text{duty}} T_{\text{inter}}) + [1 - \text{Step}(t - R_{\text{duty}} T_{\text{inter}})] \cdot (t \geq R_{\text{duty}} T_{\text{inter}}). \quad (12)$$

The function $h(X)$ describes an increasing contraction amplitude of the fish muscles from the head to the tail. To facilitate a smooth transition between the different swimming states, a step function of $\text{Step}(t)$ is applied (where both the first and second continuous derivatives exist). As shown in Fig. 4 (a), this step function makes a smooth transition from 0 to 1 over a period of time of t_a , and the reverse process can be achieved with the function of $1 - \text{Step}(t)$. Consequently, the function $s(t) = s_1(t)$ initiates the swimming from the rest to a steady swimming mode and the burst-and-coast swimming mode is achieved with the function of $s(t) = s_2(t)$ (see Fig. 4 (b)). It should be noted that a periodic extension is made for the function $s_2(t)$ within the time interval of simulation. For the function $s_2(t)$, the active muscle contractions begin to gradually reduce to 0 at the moment of t_1 , enabling a smooth transition from the burst phase to the coast phase. In the equations above, T_{inter} is the time period of the intermittent behavior, which contains a burst phase and a followed coast phase. $R_{\text{duty}} = t_1/T_{\text{inter}}$ is the duty cycle of the intermittent swimming. The grey shaded areas showed in Fig. 4 (b) denote the coast phases of the swimming.

For clarity, the key parameters of the simulation model are listed in Table 1. The mass density of the fish model is slightly larger than that of fluid. In our fish model, the fish head is totally rigid and the majority area of the fish body is covered with muscles. We set $Y_m = 0.7$ MPa, a nearly optimum stiffness value reported in (Tytell et al., 2010), as the Young's modulus of fish muscles. The authors are not aware of any direct stiffness measurements for the fish backbone. We choose the fish model of McHenry et al. (1995) as a reference and set $Y_b = 0.2$ MPa as the Young's modulus of the fish backbone. In addition, we suppose a softer caudal fin with a Young's modulus of $Y_f = 0.2$ MPa compared with the fish muscles, although Salumae and Kruusmaa (2011) have found that the fin seems to be stiffer than flesh. This is due to the fact that, in general, many carangiform fishes possess elastic membranaceous fins and the muscle stiffness can increase with the muscle activities. Like Curatolo and Teresi (2016), we set $\epsilon_{\text{max}} = 0.12$ in accordance

with the fact that the superficial fibers of a swimming fish may shorten by about 10% of their resting length. In addition, each intermittent swimming period consists of an integral number of tail beat cycles of time, which means a condition of $T_{\text{inter}} = nT$ (where n is an integer).

3. Results and discussion

3.1. Grid independence test

Prior to conducting a detailed simulation study, the tests of grid and time resolution independence are conducted. A steady swimming case with $f = 4$ Hz, $\lambda = L$, $n = 10$ and $R_{\text{duty}} = 0.5$ is considered. As shown in Table 2, three different mesh densities are selected. Two temporal resolutions are chosen as $\Delta t_1 = T/500$ and $\Delta t_2 = T/800$. To catch the swimming details more accurately, the finest mesh elements are close to the fish boundary for all the three mesh cases. Fig. 5 (a) shows the comparison of the transient swimming velocity of fish (v) during the whole duration of simulation. In addition, it is generally acknowledged that the caudal fin has a great effect on the swimming performance of fish. Therefore, we also compare the motion trajectories of the caudal fin tip. Fig. 5 (b) gives the variations of y_{fintip} (the Y coordinate of the caudal fin tip) with time for all the cases. There are no significant differences between the results of the medium mesh (mesh b) and the fine mesh (mesh c) under the condition of Δt_1 . In addition, for the mesh b, the results of the two temporal resolutions are in good agreement. Eventually, the mesh b and the time resolution $\Delta t_1 = T/500$ (500 steps per tail beat period) are adopted in the following simulations.

3.2. Post processing

We will examine and compare the swimming hydrodynamic forces and the energy expenditures of the two swimming modes. By integrating the components of normal stress on the FSI boundary, we can get the net forces exerted by the fish on the fluid:

$$F_j^{\text{net}} = \int_{\partial\Omega_{\text{st}}} (-p\mathbf{I} + \mathbf{K})\mathbf{n} \cdot \mathbf{e}_j ds, \quad j = 1, 2. \quad (13)$$

In this equation, the values of subscript $j = 1, 2$ represent the

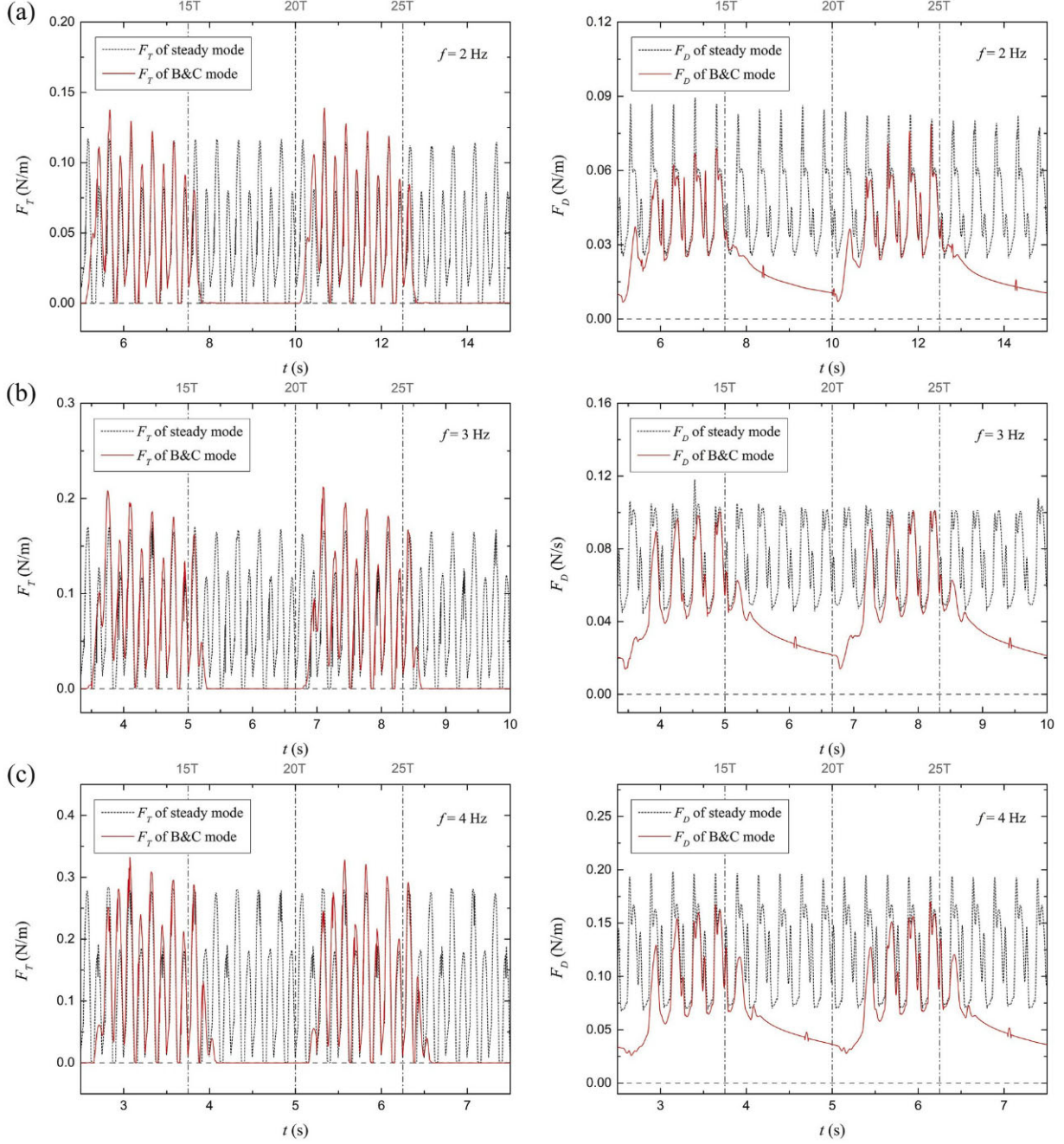


Fig. 8. Time histories of the instant thrusts and drags of the intermittent swimming mode (B&C mode) and the steady swimming mode (steady mode). (a) $f = 2$ Hz. (b) $f = 3$ Hz. (c) $f = 4$ Hz.

components in X and Y directions, respectively. The parameter \mathbf{e}_j denotes the unit vectors in the direction of coordinate axes. We decompose the net forces as follows (Borazjani and Sotiropoulos, 2008):

$$F_{Tj} = \frac{1}{2} (F_j^{net} + f_j), \quad F_{Dj} = \frac{1}{2} (-F_j^{net} + f_j), \quad (14)$$

$$f_j = \left| \int_{\partial\Omega_{st}} p\mathbf{n} \cdot \mathbf{e}_j ds \right| + \left| \int_{\partial\Omega_{st}} \mathbf{K}\mathbf{n} \cdot \mathbf{e}_j ds \right|, \quad (15)$$

where F_{Tj} and F_{Dj} are the thrust and drag components, respectively. The swimming direction is assessed by computing the average horizontal component of fluid velocity v_1 on the FSI boundary:

$$\theta = \frac{1}{L_b} \int_{\partial\Omega_{st}} a \cos\left(\frac{v_1}{|\mathbf{v}|}\right) ds, \quad (16)$$

where L_b is the fish contour length. Therefore, the net force F^{net} , the thrust force F_T , and the drag force F_D along the swimming direction can be calculated as follows:

$$\begin{cases} F^{net} = F_1^{net} \cos(\theta) + F_2^{net} \cos(\pi/2 - \theta) \\ F_T = F_{T1} \cos(\theta) + F_{T2} \cos(\pi/2 - \theta) \\ F_D = F_{D1} \cos(\theta) + F_{D2} \cos(\pi/2 - \theta) \end{cases} . \quad (17)$$

Obviously, these three forces have the following relationship:

$$F^{net} = F_T - F_D. \quad (18)$$

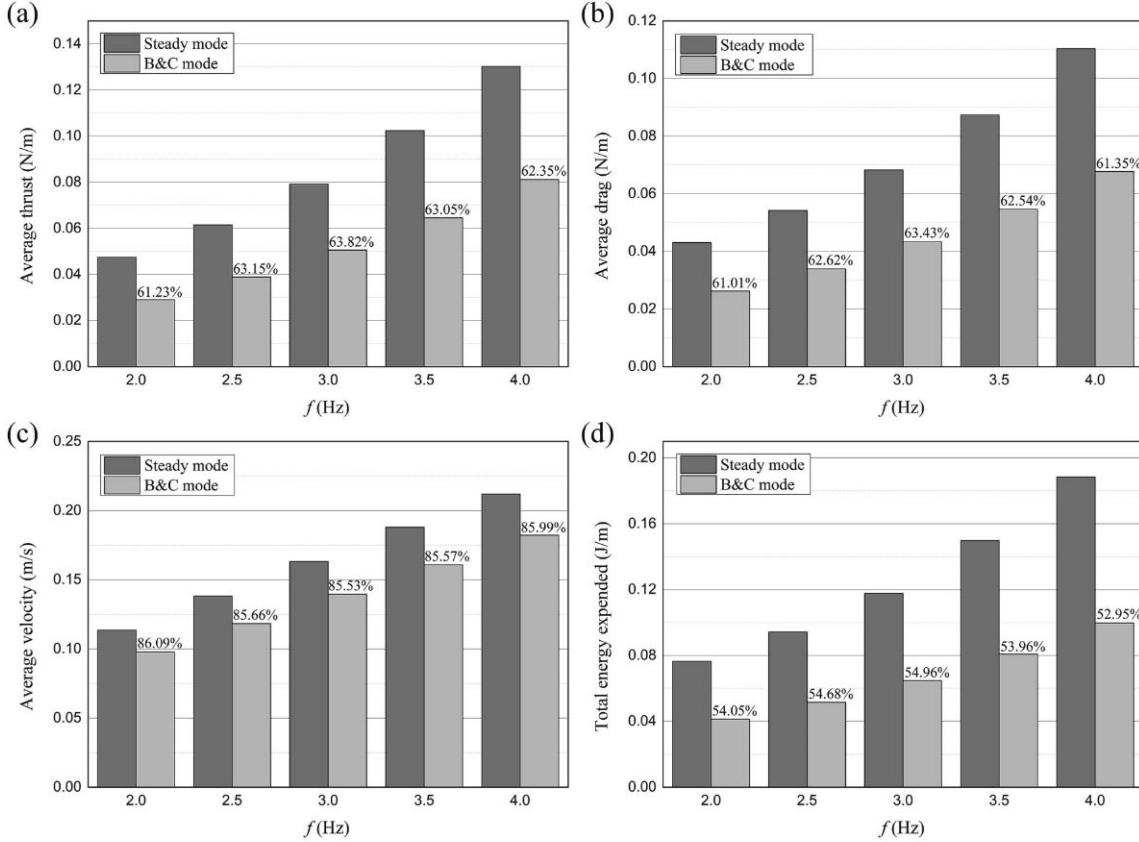


Fig. 9. Histograms of the key features of swimming performance for the intermittent swimming mode (B&C mode) and the steady swimming mode (steady mode).

The energy expenditure over a burst-and-coast swimming cycle is calculated as (Fish et al., 1991):

$$W_{bc} = W_b + W_c, \quad (19)$$

where W_b and W_c are the energy expended during the burst phase and the coast phase, respectively. The rate of energy expended for a body moving through water is equal to the product of the drag force and the velocity (Fish et al., 1991), the equation (19) can be rewritten as:

$$W_{bc} = \int_{t_0}^{R_{duty}-T_{\text{inter}}} F_D v dt + \int_{R_{duty}-T_{\text{inter}}}^{T_{\text{inter}}} F_D v dt, \quad (20)$$

where t_0 is the starting time of a burst phase and v is the fish swimming velocity. Three non-dimensional parameters related to the fish swimming are the Reynolds number (Re), the swimming number (Sw) and the Strouhal number (St), which are defined as follows:

$$Re = \frac{v_{\text{swim}} L \rho_f}{\mu}, \quad Sw = \frac{A \omega L \rho_f}{\mu}, \quad St = \frac{Af}{v_{\text{swim}}}, \quad (21)$$

where v_{swim} is the average swimming velocity of the fish over a tail beat cycle and A is the total excursion of the caudal fin from one side to the other over a tail beat cycle. To compare the two swimming modes, three parameters are introduced, the ratio of the total energy expenditure (C_w), the ratio of the average swimming velocity and the ratio of C_v to C_w (δ), which are defined as follows:

$$C_w = \frac{W_{BC}}{W_{\text{Steady}}}, \quad C_v = \frac{\bar{v}_{BC}}{\bar{v}_{\text{Steady}}}, \quad \delta = \frac{C_v}{C_w}, \quad (22)$$

where W_{BC} and W_{Steady} are the total energy expenditures of the burst-and-coast swimming mode and the relevant steady swimming mode over the whole simulation process, respectively. \bar{v}_{BC} and \bar{v}_{Steady} are the

average swimming velocities of the two swimming modes over the whole simulation process. In general, the coast swimming will result in a velocity loss and an energy saving compared with the steady swimming. Consequently, a higher value of C_v indicates a less velocity loss and a smaller value of C_w means a less energy expenditure for the burst-and-coast swimming, while δ is a comprehensive parameter including the two aspects.

3.3. Benefits of intermittent swimming

Before going further, we first take a quick look at the result of the intermittent swimming simulation. Fig. 6 shows the instantaneous vorticity fields of a burst-and-coast swimming case with $f = 4$ Hz, $\lambda = L$, $T_{\text{inter}} = 10T$, and $R_{\text{duty}} = 0.5$. The related animations of the burst-and-coast swimming simulation and the relevant steady swimming simulation can be found on-line in the supplementary movies as Movie S1 and Movie S2, respectively. In Fig. 6 (a), the fish starts to undulate its body and tail from the resting state. Consequently, with the active undulations, the fish swims forward successfully (see Fig. 6 (b)). After a burst phase down, the fish begin to coast in Fig. 6 (c). Fish straightens its body and glides forward without muscle activities in the coast phase (see Fig. 6 (d)). Then, the fish enters into a new burst phase and continues to swim forward (see Fig. 6 (e) and (f)). As shown in Fig. 6, the vorticity field is depicted and the motion trajectory of the caudal fin tip is also plotted with a black solid line. The clockwise and counterclockwise vorticity values are plotted in blue and red, respectively. A typical reversed Von Karman vortex pattern can be clearly observed only in the wake of the burst phases. Compared with the steady swimming, the main feature of the burst-and-coast swimming is that the reversed Von Karman vortex pattern appears intermittently. Fish strives to propel itself forward by undulating its body and caudal fin to push the adjacent water downward at the burst phases, and then glides forward relying on

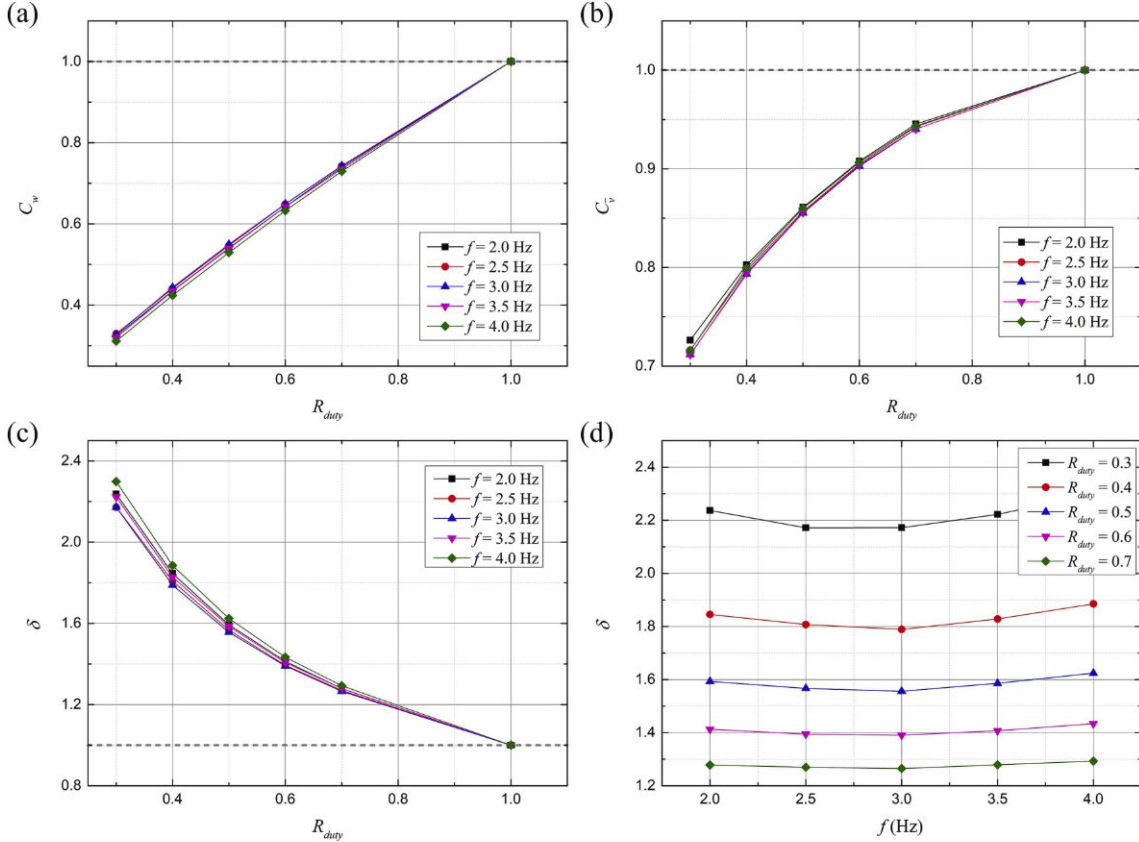


Fig. 10. Effect of the duty cycle (R_{duty}) on the performance of intermittent swimming. (a) The variation of C_w versus R_{duty} . (b) The variation of C_v versus R_{duty} . (c) The variation of δ versus R_{duty} . (d) The variation of δ versus f .

inertia at the coast phases. It should be noted that the swimming of the fish model is not perfectly horizontal from the left to right. This is because the influences of the initial disturbances and the mesh asymmetries are inevitable, and there is no any direction control scheme in the present simulations.

Supplementary data related to this article can be found at <https://doi.org/10.1016/j.oceaneng.2020.107391>.

To evaluate the potential benefits of intermittent swimming, a comparative study of the intermittent swimming and the steady swimming is conducted in the tail beat frequency range of $f = 2$ Hz~4 Hz. Each simulation trial consists of 30 tail beat cycles with $\lambda = L$, $T_{inter} = 10T$, and $R_{duty} = 0.5$. Fig. 7 shows the time histories of the swimming velocity of the intermittent swimming and the relevant steady swimming. A similar change tendency of the swimming velocity is showed for all the three tail beat frequencies. For the steady swimming mode, the fish accelerates to swim forward and eventually reaches a constant average velocity, in spite of the fluctuation in each tail beat cycle. In contrast, for the intermittent swimming mode, a deceleration process can be observed in the coast phase, and then an acceleration process is followed during the next burst phase. This variation pattern of the swimming velocity coincides with the description of Videler and Weis (1982) and the simulation results of Akoz and Moored (2017). Moreover, with the tail beat frequency increase, both the acceleration and the final average swimming velocity of the steady mode are increased. Fig. 8 gives the time histories of the instant thrust force and drag force for the three tail beat frequencies. For clarity, only the data of the last two time periods of intermittent swimming are plotted. Compared with the steady swimming mode, with the absence of active muscle movements, the thrust force reduces to zero during the coast phases. At the same time, the drag force is significantly less than that of the steady swimming mode and it decreases with the drop of swimming velocity. This result

conforms to the reality that the drag of an undulating fish body is greater than the drag of a coasting fish (Lighthill, 1971). On the other hand, the thrust force of the burst phase is much greater than the drag force, resulting in the acceleration process (see Fig. 7). During the burst phase, with the increase of swimming velocity, the drag force increases and the thrust force decreases.

Furthermore, the bar graphs seen in Fig. 9 show the comparison of the average thrust, the average drag, the average velocity and the total energy expended of the two swimming modes over the whole simulation process. For each value, the proportion of the result of intermittent swimming to that of the steady swimming is given. As shown in Fig. 9 (a) and (b), the average thrust force and drag force for the two swimming modes are both increased with the tail beat frequency. Compared with the steady mode, a same percentage of nearly 37% decrease in the average thrust and drag forces can be found by the intermittent swimming. In addition, we calculate the average swimming velocity based on the total swimming displacement and give the total energy expended over the whole simulation process. The average swimming velocity almost scale linearly with the tail beat frequency (see Fig. 9 (c)). It is reasonable to assume that the fish tries to get a higher swimming speed with a less energy expenditure. However, the energy saving and the speed increase are often in conflict with each other. As a consequence, we have reasons to believe that there will be a tradeoff between these two aspects. This may partly explain why the fish have to develop so many swimming patterns and switch freely between them. As can be seen from Fig. 9 (c) and (d), a nearly 46% energy saving can be achieved by the intermittent swimming over the whole simulation process. At the same time, the energy saving is accompanied by a nearly 14% of speed droop. In general, if the swimming speed is not a priority, it will pay to sacrifice a little speed for the huge energy saving.

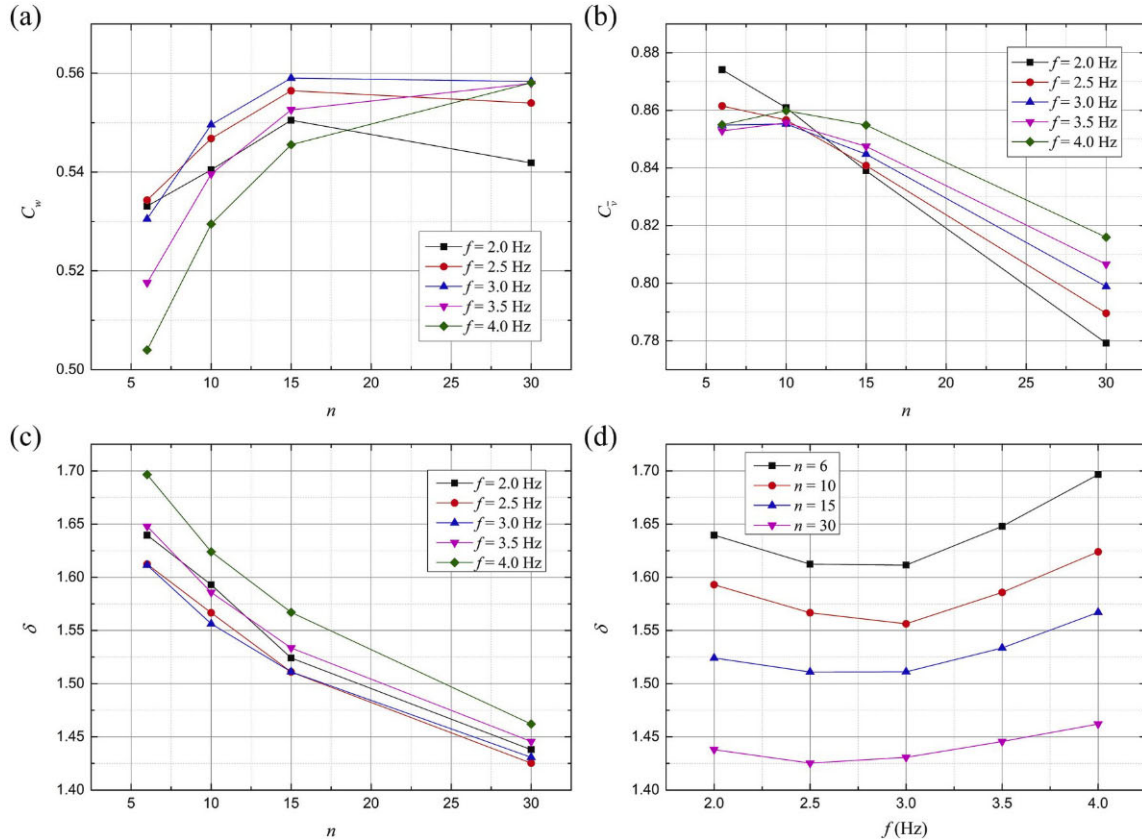


Fig. 11. Effect of the tail swing number in a burst phase on the performance of intermittent swimming. (a) The variation of C_w versus n . (b) The variation of C_v versus n . (c) The variation of δ versus n . (d) The variation of δ versus f .

Table 3
Values of the Strouhal number St of steady swimming for some pairs (f, λ) .

f	$\lambda/L = 1$	$\lambda/L = 2$	$\lambda/L = 3$
2 Hz	0.529	0.599	0.651
3 Hz	0.477	0.646	0.721
4 Hz	0.463	0.705	0.809

3.4. Effect of the duty cycle

In this subsection, the effect of the duty cycle (R_{duty}) on the performance of intermittent swimming will be investigated. The duty cycle is varied from 0.3 to 0.7 every 0.1, and all other simulation conditions remain unchanged with that of the previous subsection. It is worth noting that the steady swimming can be regarded as a special case of intermittent swimming with $R_{duty} = 1$. The effects of duty cycle on the parameters C_w , C_v and δ are presented in Fig. 10. As shown in Fig. 10 (a) and (b), both the energy expenditure and the average swimming velocity of the intermittent swimming are increased with the increase of duty cycle. As can be seen, the fish swimming can be gradually transited from an intermittent mode to the continuous mode by increasing the duty cycle. As shown in Fig. 10 (c), the parameter δ (the ratio of C_v to C_w)

decreases with the duty cycle. A higher value of δ is considered beneficial in improving the energy utilization rate, which means less energy consumption up to a certain swimming velocity. A smaller duty cycle means a longer glide time. As a result, the fish can save more energy to obtain the same swimming velocity. This is in accordance with the simulation results of Xia et al. (2018). In a word, if the swimming speed is not a priority, a smaller duty cycle will be a better choice to save more energy by coasting more time. Moreover, for the different values of duty cycle, the change curves of δ accompanied with the tail beat frequency are drawn in Fig. 10 (d). Compared with the higher and the lower frequencies, the values of δ are smaller at the moderate frequencies. This phenomenon is more obvious at the smaller duty cycle.

3.5. Effect of the tail swing number in a burst phase

In this paper, the intermittent swimming of fish is considered as a cyclical behavior with a time period of $T_{inter} = nT$. All the simulation results showed above are based on the condition of $T_{inter} = 10T$, and that means each intermittent swimming period consists of 10 tail beat cycles of time. Wu et al. (2007) have found that the carps have two burst modes: the multiple tail-beat mode (MT mode) and the half tail-beat mode (HT mode). For the first mode, the fish tail beats for at least one cycle in the burst phase, by contrast, the tail beats for only a half-cycle

Table 4
Values of the non-dimensional parameter pairs (Sw, Re) of steady swimming for some pairs (f, λ) .

f	$\lambda/L = 1$	$\lambda/L = 2$	$\lambda/L = 3$
2 Hz	$(4.21 \times 10^4, 1.27 \times 10^4)$	$(5.34 \times 10^4, 1.42 \times 10^4)$	$(5.77 \times 10^4, 1.41 \times 10^4)$
3 Hz	$(5.57 \times 10^4, 1.86 \times 10^4)$	$(8.06 \times 10^4, 1.98 \times 10^4)$	$(8.79 \times 10^4, 1.93 \times 10^4)$
4 Hz	$(7.14 \times 10^4, 2.45 \times 10^4)$	$(1.06 \times 10^5, 2.39 \times 10^4)$	$(1.15 \times 10^5, 2.25 \times 10^4)$

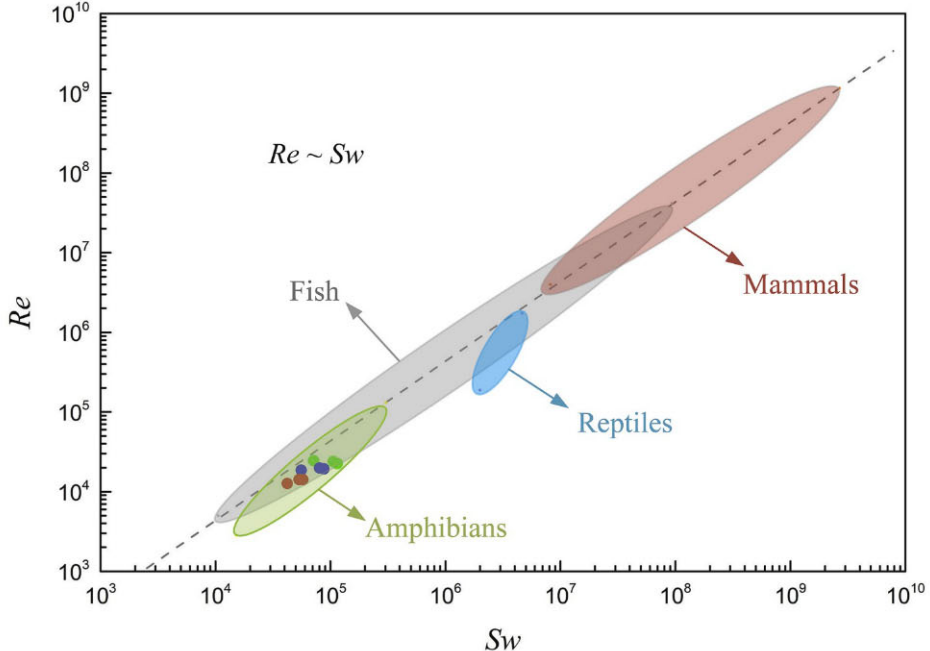


Fig. 12. Comparison with the scaling relation of $Re \sim Sw$ proposed by Gazzola et al. (2014). The colored circles, red, blue and green, refer to the results (listed in Table 4) with $f = 2$ Hz, $f = 3$ Hz and $f = 4$ Hz, respectively. (For interpretation of the references to color in this figure legend, the reader is referred to the Web version of this article.)

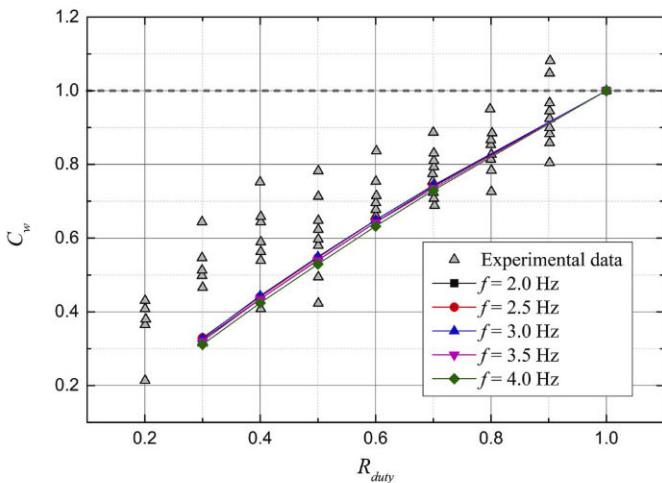


Fig. 13. Qualitative comparison of the computed energy expended ratio C_w with the experimental data of Floryan et al. (2017).

for the second mode. Obviously, the present simulations of the intermittent swimming are belong to the MT mode. In order to investigate the effect of the tail swing number in a burst phase on the swimming performance, four different values of the coefficient n (i.e., $n = 6, 10, 15$ and 30) are considered under the conditions of $\lambda = L$ and $R_{duty} = 0.5$. Consequently, the fish swings its tail for 3, 5, 7.5 and 15 times in each burst phase, respectively. As shown in Fig. 11 (a), the energy expenditures increase monotonically with n for the higher tail beat frequencies. A further increase of n actually reduces the energy expenditures for the lower tail beat frequencies. In contrast, the average swimming velocities decrease with n and the change curve of C_w has an anti-clockwise rotation with the increase of tail beat frequency (see Fig. 11 (b)). As shown in Fig. 11 (c), the parameter δ decreases with n for all the tail beat frequencies. Therefore, in the range considered, the smaller value of n is, the higher energy utilization rate is. Compared with the Figs. 10 (d),

Fig. 11 (d) shows a same phenomenon that the moderate tail beat frequencies may result in a lower energy utilization rate. As described above, the average swimming velocity almost scale linearly with the tail beat frequency. An assumption can be inferred that the intermittent swimming will have more benefits at the lower and the higher swimming speeds.

3.6. Comparison with the real swimmers

In this subsection, the results of present swimming simulation will be compared with that of the previous studies. For the steady swimming, the values of the Strouhal number (St), the Reynolds number (Re) and the swimming number (Sw) for some pairs of (f, λ) are listed in Table 3 and Table 4. All the values are calculated when the acceleration period has terminated. As shown in Table 3, higher values of wavelength (λ) seem to produce a greater Strouhal number, which is in accordance with the result of Curatolo and Teresi (2016). As for the Reynolds number (Re) and the swimming number (Sw), both parameters are increased with the tail beat frequency. The Reynolds number for the swimmers can be assumed to be proportional to the swimming number (Gazzola et al., 2014). As shown in Fig. 12, the dashed line represents the proportional relation of $Re \sim Sw$ proposed by Gazzola et al. (2014). The ranges of Re and Sw for the four different genera of swimmer in the turbulent regime are depicted based on the measurements of Gazzola et al. (2014). The results of Re and Sw showed in Table 4 are also plotted, which show a good agreement with the proportional relation. For the intermittent swimming, we consider a water tunnel experiment on a nominally two-dimensional pitching foil conducted by Floryan et al. (2017). They investigated the intermittent propulsion of a rigid pitching foil to understand the fish intermittent swimming behavior. Fig. 13 shows the qualitative comparison of the computed energy expended ratio C_w with the experimental data of Floryan et al. (2017). As shown in Fig. 13, the varying trend of computed C_w is consistent with the experimental data. According to the literature (Videler and Weihs, 1982), the cod frequently use the steady swimming at velocities between 1.4 BL/s (i.e., body lengths per second) and 2 BL/s, and an intermittent swimming below 1.4 BL/s. At average velocities higher than 2.5 BL/s, the

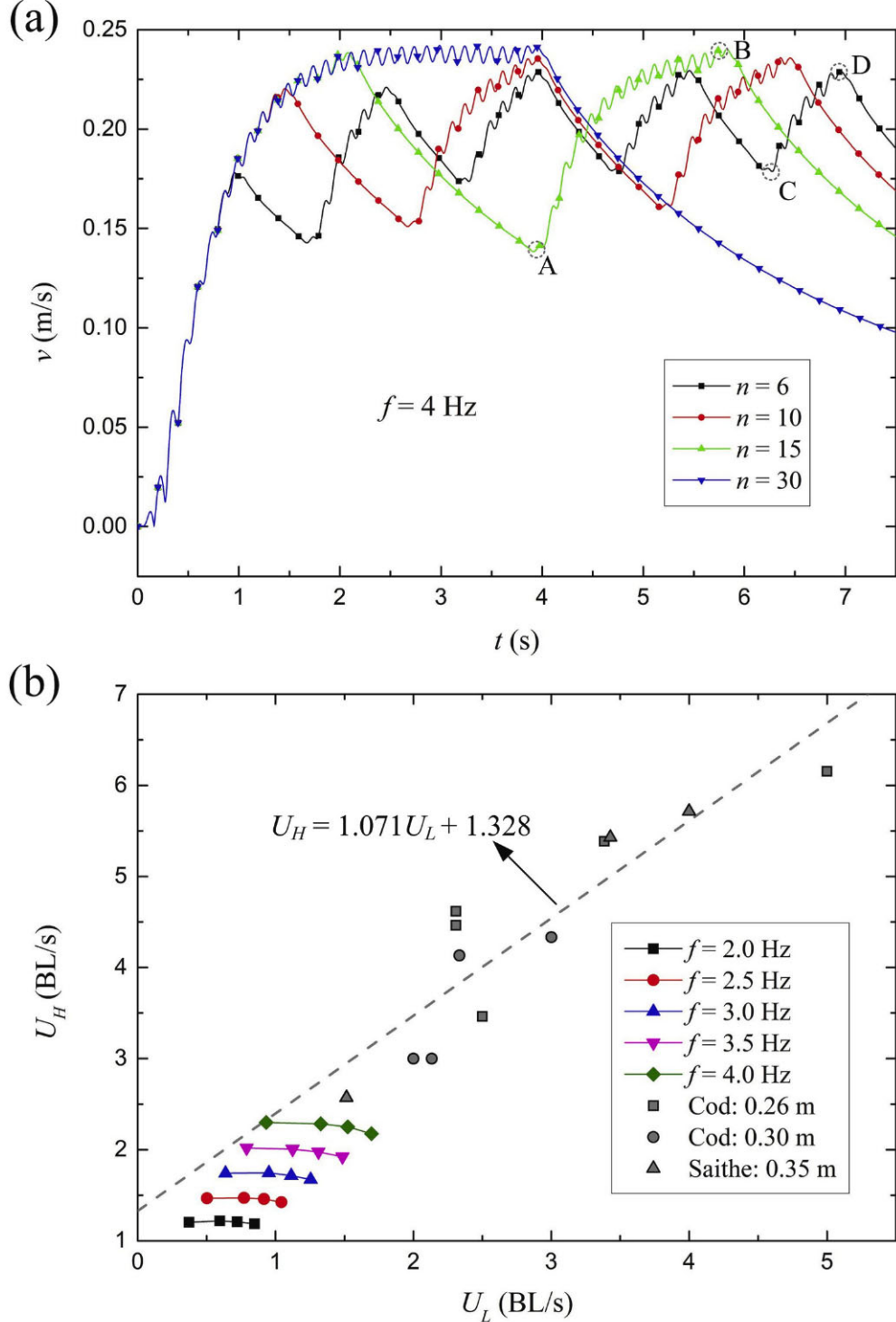


Fig. 14. (a) The time histories of the transient swimming velocity for different values of n under the condition of $f = 4$ Hz. (b) The linear regression analysis of the measured data of U_L (BL/s) and U_H (BL/s) for the cod and saithe (Videler and Weihs, 1982).

intermittent swimming is again the usual mode and the steady swimming is occasionally observed. Saithe exhibit a similar behavior under the same circumstances. The proposed assumption that the intermittent swimming have more benefits at the lower and the higher swimming speeds illustrated above may partly explain this phenomenon. For the effect of the coefficient n , Fig. 14 (a) shows the time histories of the transient swimming velocity under the condition of $f = 4$ Hz. Within the same amount of simulation time, the number of intermittent swimming cycles is decreased with the increase of n . The transient

swimming velocity has two bounds. The lower bound (U_L) represents the initial velocity of a burst phase (e.g. point A and C) and the upper bound (U_H) represents the final velocity of a burst phase (e.g. point B and D). As shown in Fig. 14 (a), with the increase of n , U_H increases, while U_L decreases. Fig. 14 (b) gives the measured data of U_L (BL/s) and U_H (BL/s) for the cod and saithe (Videler and Weihs, 1982). Through the linear regression analysis, we obtain a fitted curve ($U_H = 1.071U_L + 1.328$), giving a Pearson correlation coefficient value of 0.897 and an R-square value of 0.786. Therefore, U_H is almost linear with U_L in the intermittent

swimming of live fish. The results of U_L and U_H for the simulations showed in Fig. 11 are also plotted. For the five clusters correspond to different frequencies, the biases of the results from the fitted curve are increased with the increase of n from left to right. Combined with the previous content, it can be concluded that a proper proportion of the velocity bounds is very important for the performance improvement of the intermittent swimming.

4. Conclusions

In this work, we have modeled and studied the intermittent swimming gait of a 2D carangiform fish with the muscle-contraction model of pre-strains. A comparative study of the intermittent swimming and the steady swimming was conducted to evaluate the potential benefits of the intermittent swimming. We compared the hydrodynamic forces, swimming velocities and the energy expended of these two swimming modes during the whole simulation process. We assumed that the fish tries to get a higher swimming speed with a less energy expenditure. However, simulation results showed that the energy saving and the speed increase are often in conflict with each other. Fish can reduce the energy consumption for swimming by using the intermittent gait. At the same time, however, the average swimming velocity is inevitably reduced. So, we proposed an assumption that fish have to make a tradeoff between the energy saving and the gain of swimming speed. This may partly explain why fish have to develop so many swimming patterns and switch freely between them.

We studied the effects of the duty cycle of intermittent swimming on the swimming performance. The results showed that both the energy expenditure and the average swimming velocity are increased with the increase of duty cycle. The fish swimming can be gradually transited from an intermittent mode to the continuous mode by increasing the duty cycle. In addition, we also considered the effect of the tail swing number in a burst phase on the swimming performance. We found that a smaller tail swing number in a burst phase is more helpful to improve the energy utilization rate under the condition of $R_{duty} = 0.5$. Moreover, the intermittent swimming will have more benefits at the lower and the higher swimming speeds. A proper proportion of the velocity bounds is very important for the performance improvement of the intermittent swimming. These conclusions may have direct meanings for the development of AUVs.

It should be noted that there are limitations to this 2D simulation study. The muscles of fish may have two principal types: the red muscles and the white muscles. We did not perform a functional segmentation of the fish muscles. However, different muscle types may have different mechanical and energetic properties, and thus affect the swimming performance. In addition, the three-dimensional effects of the fish body on the performance of intermittent swimming need to be studied in future works.

Declaration of interest statement

The authors declare that they have no known competing financial interests or personal relationships that could have appeared to influence the work reported in this paper.

CRediT authorship contribution statement

Zhijie Zhao: Investigation, Methodology, Writing - original draft, Writing - review & editing. **Lei Dou:** Funding acquisition, Resources, Project administration.

Acknowledgements

This work was financially supported by the National Natural Science Foundation of China (grant 60904085), Foundation of National Key Laboratory of Transient Physics, and Foundation of Defence Technology

Innovation Special Filed.

References

- Akoz, E., Moored, K., 2017. Unsteady propulsion by an intermittent swimming gait. *J. Fluid Mech.* 834, 149–172. <https://doi.org/10.1017/jfm.2017.731>.
- Altringham, J.D., Ellerby, D., 2000. Fish swimming: patterns in muscle function. *J. Exp. Biol.* 202, 3397–3403.
- Bao, Y., Zhou, D., Tao, J., Peng, Z., Zhu, H., Sun, Z.L., Tong, H.L., 2017. Dynamic interference of two anti-phase flapping foils in side-by-side arrangement in an incompressible flow. *Phys. Fluids* 29 (33601). <https://doi.org/10.1063/1.4978301>.
- Borazjani, I., Sotiropoulos, F., 2008. Numerical investigation of the hydrodynamics of carangiform swimming in the transitional and inertial flow regimes. *J. Exp. Biol.* 211, 1541–1558. <https://doi.org/10.1242/jeb.015644>.
- Calovi, D., Litchinko, A., Lecheval, V., Lopez, U., Pérez Escudero, A., Chaté, H., Sire, C., Theraulaz, G., 2017. Disentangling and Modeling Interactions in Fish with Burst-And-Coast Swimming.
- Chan, W.L., Kang, T., Lee, Y.J., 2007. Experiments and identification of an ostraciform fish robot. In: 2007 IEEE International Conference on Robotics and Biomimetics (ROBIO), pp. 530–534. <https://doi.org/10.1109/ROBIO.2007.4522218>.
- Chang, X., Zhang, L., He, X., 2012. Numerical study of the thunniform mode of fish swimming with different Reynolds number and caudal fin shape. *Comput. Fluids* 68, 54–70. <https://doi.org/10.1016/j.compfluid.2012.08.004>.
- Costa, D., Franciolini, M., Palmieri, G., Crivellini, A., Scaradozzi, D., 2017. Computational fluid dynamics analysis and design of an ostraciform swimming robot. In: 2017 IEEE International Conference on Robotics and Biomimetics (ROBIO), pp. 135–140. <https://doi.org/10.1109/ROBIO.2017.8324407>.
- Costa, D., Callegari, M., Palmieri, G., Scaradozzi, D., Brocchini, M., Zitti, G., 2018. Experimental setup for the validation of the bio-inspired thruster of an ostraciform swimming robot. 2018 14th IEEE/ASME International Conference Mechatronic Embedded System Applications. MESA 2018, pp. 1–6. <https://doi.org/10.1109/MESA.2018.8449165>.
- Costa, D., Palmieri, G., Scaradozzi, D., Callegari, M., 2019. Multi-body analysis of a bio-inspired underwater robot. In: Carbone, G., Gasparetto, A. (Eds.), *Advances in Italian Mechanism Science*. Springer International Publishing, Cham, pp. 240–248.
- Curatolo, M., Teresi, L., 2016. Modeling and simulation of fish swimming with active muscles. *J. Theor. Biol.* 409, 18–26. <https://doi.org/10.1016/j.jtbi.2016.08.025>.
- Deng, J., Shao, X., Ren, A., 2006. Numerical study on propulsive performance of fish-like swimming foils. *J. Hydronaut. Ser. B* 18, 681–687. [https://doi.org/10.1016/S1001-6058\(07\)60007-9](https://doi.org/10.1016/S1001-6058(07)60007-9).
- Evangelista, A., Nardinocchi, P., Puddu, P.E., Teresi, L., Torromeo, C., Varano, V., 2011. Torsion of the human left ventricle: experimental analysis and computational modeling. *Prog. Biophys. Mol. Biol.* 107, 112–121. <https://doi.org/10.1016/j.pbiomolbio.2011.07.008>.
- Fish, F.E., Fegely, J.F., Xanthopoulos, C.J., 1991. Burst-and-coast swimming in schooling fish (*Notemigonus crysoleucas*) with implications for energy economy. *Comp. Biochem. Physiol. Part A Physiol* 100, 633–637. [https://doi.org/10.1016/0300-9629\(91\)90382-M](https://doi.org/10.1016/0300-9629(91)90382-M).
- Flammang, B., Lauder, G., 2009. Caudal fin shape modulation and control during acceleration, braking and backing maneuvers in bluegill sunfish, *Lepomis macrochirus*. *J. Exp. Biol.* 212, 277–286. <https://doi.org/10.1242/jeb.021360>.
- Floryan, D., Van Buren, T., Smits, A., 2017. Forces and energetics of intermittent swimming. *Acta Mech. Sin.* 33, 725–732. <https://doi.org/10.1007/s10409-017-0694-3>.
- Gao, A., Triantafyllou, M.S., 2018. Independent caudal fin actuation enables high energy extraction and control in two-dimensional fish-like group swimming. *J. Fluid Mech.* 850, 304–335. <https://doi.org/10.1017/jfm.2018.456>.
- Gazzola, M., Argentina, M., Mahadevan, L., 2014. Scaling macroscopic aquatic locomotion. *Nat. Phys.* 10, 758–761. <https://doi.org/10.1038/nphys3078>.
- Gleiss, A., Jorgensen, S., Liebsch, N., Sala, J., Norman, B., Hays, G., Quintana, F., Grundy, E., Campagna, C., Trites, A., Block, B., 2011. Convergent evolution in locomotory patterns of flying and swimming animals. *Nat. Commun.* 2 (352) <https://doi.org/10.1038/ncomms1350>.
- COMSOL Inc, 2018. COMSOL documentation.
- Iosilevskii, G., 2016. Locomotion of neutrally buoyant fish with flexible caudal fin. *J. Theor. Biol.* 399, 159–165. <https://doi.org/10.1016/j.jtbi.2016.04.001>.
- Jayne, B., Lauder, G., 1994. How swimming fish use slow and fast muscle fibers: implications for models of vertebrate muscle recruitment. *J. Comp. Physiol. A* 175, 123–131. <https://doi.org/10.1007/BF00217443>.
- Karbasian, H.R., Esfahani, J.A., 2017. Enhancement of propulsive performance of flapping foil by fish-like motion pattern. *Comput. Fluids* 156, 305–316. <https://doi.org/10.1016/j.compfluid.2017.07.016>.
- Li, C., Yang, W., Xu, X., Wang, J., Wang, M., Xu, L., 2017. Numerical investigation of fish exploiting vortices based on the Kármán gaiting model. *Ocean Eng.* 140, 7–18. <https://doi.org/10.1016/j.oceaneng.2017.05.011>.
- Lighthill, M., 1971. Large-amplitude elongated-body theory of fish locomotion. *Proc. R. Soc. Lond. Ser. B Biol. Sci.* 179, 125–138. <https://doi.org/10.1098/rspb.1971.0085>.
- McHenry, M., Pell, C., Long Jr., J., 1995. Mechanical control of swimming speed: stiffness and axial wave form in undulating fish models. *J. Exp. Biol.* 198, 2293–2305.
- Müller, U., Stamhuis, E.J., Videler, J., 2000. Hydrodynamics of unsteady fish swimming and the effects of body size: comparing the flow fields of fish larvae and adults. *J. Exp. Biol.* 203, 193–206.

- Mwaffo, V., Zhang, P., Cruz, S., Porfiri, M., 2017. Zebrafish swimming in the flow: a particle image velocimetry study. *PeerJ* 5, e4041. <https://doi.org/10.7717/peerj.4041>.
- Nardinocchi, P., Teresi, L., 2007. On the active response of soft living tissues. *J. Elasticity* 88, 27–39. <https://doi.org/10.1007/s10659-007-9111-7>.
- Nardinocchi, P., Teresi, L., 2013. Electromechanical modeling of anisotropic cardiac tissues. *Math. Mech. Solid* 18, 576–591. <https://doi.org/10.1177/1081286513485774>.
- Nardinocchi, P., Teresi, L., Varano, V., 2013. The elastic metric: a review of elasticity with large distortions. *Int. J. Non Lin. Mech.* 56, 34–42. <https://doi.org/10.1016/j.ijnonlinmec.2013.05.002>.
- Pavlov, V., Rosental, B., Hansen, N.F., Beers, J., Parish, G., Rowbotham, I., Block, B.A., 2017. Hydraulic control of tuna fins: a role for the lymphatic system in vertebrate locomotion. *Science* 357, 310–314. <https://doi.org/10.1126/science.aak9607>.
- Rayner, J., Viscardi, P., Ward, S., Speakman, J., 2001. Aerodynamics and energetics of intermittent flight in birds. *Am. Zool.* 41, 188–204. <https://doi.org/10.1093/icb/41.2.188>.
- Ren, Z., Yang, X., Wang, T., Wen, L., 2016. Hydrodynamics of a robotic fish tail: effects of the caudal peduncle, fin ray motions and the flow speed. *Bioinspiration Biomimetics* 11 (16008). <https://doi.org/10.1088/1748-3190/11/1/016008>.
- Ribak, G., Weihs, D., Arad, Z., 2005. Submerged swimming of the great cormorant *Phalacrocorax carbo sinensis* is a variant of the burst-and-glide gait. *J. Exp. Biol.* 208, 3835–3849. <https://doi.org/10.1242/jeb.01856>.
- Rome, L.C., Funke, R.P., Alexander, R.M., Lutz, G., Aldridge, H., Scott, F., Freedman, M., 1988. Why animals have different muscle fibre types. *Nature* 335, 824–827. <https://doi.org/10.1038/335824a0>.
- Rome, L., Swank, D., Corda, D., 1993. How fish power swimming. *Science* 261, 340–343. <https://doi.org/10.1126/science.8332898>.
- Salumae, T., Kruusmaa, M., 2011. A flexible fin with bio-inspired stiffness profile and geometry. *J. Bionic Eng* 8, 418–428. [https://doi.org/10.1016/S1672-6529\(11\)60047-4](https://doi.org/10.1016/S1672-6529(11)60047-4).
- Scaradozzi, D., Palmieri, G., Costa, D., Pinelli, A., 2017. BCF swimming locomotion for autonomous underwater robots: a review and a novel solution to improve control and efficiency. *Ocean Eng.* 130, 437–453. <https://doi.org/10.1016/j.oceaneng.2016.11.055>.
- Shaw, J.A., Dasharathi, K., Wineman, A.S., Si, M.-S., 2015. A simple model for myocardial changes in a failing heart. *Int. J. Non Lin. Mech.* 68, 132–145. <https://doi.org/10.1016/j.ijnonlinmec.2014.06.015>.
- Sun, P.-N., Colagrossi, A., Zhang, A.-M., 2018. Numerical simulation of the self-propulsive motion of a fishlike swimming foil using the δ^+ -SPH model. *Theor. Appl. Mech. Lett.* 8, 115–125. <https://doi.org/10.1016/j.taml.2018.02.007>.
- Takagi, T., Tamura, Y., Weihs, D., 2013. Hydrodynamics and energy-saving swimming techniques of Pacific bluefin tuna. *J. Theor. Biol.* 336, 158–172. <https://doi.org/10.1016/j.jtbi.2013.07.018>.
- Tobalske, W.B., 2001. Morphology, velocity, and intermittent flight in birds. *Am. Zool.* 41, 177–187. <https://doi.org/10.1093/icb/41.2.177>.
- Tobalske, W.B., Hearn, J.W.D., Warrick, D.R., 2010. Aerodynamics of intermittent bounds in flying birds. *Exp. Fluid* 46, 963–973. <https://doi.org/10.1007/s00348-009-0614-9>.
- Tytell, E.D., Hsu, C.Y., Williams, T.L., Cohen, A.H., Fauci, L.J., 2010. Interactions between internal forces, body stiffness, and fluid environment in a neuromechanical model of lamprey swimming. *Proc. Natl. Acad. Sci. U. S. A* 107, 19832–19837. <https://doi.org/10.1073/pnas.1011564107>.
- Videler, J., Weihs, D., 1982. Energetic advantages of burst-and-coast swimming of fish at high speeds. *J. Exp. Biol.* 97, 169–178.
- Weihs, D., 1974. Energetic advantages of burst swimming of fish. *J. Theor. Biol.* 48, 215–229. [https://doi.org/10.1016/0022-5193\(74\)90192-1](https://doi.org/10.1016/0022-5193(74)90192-1).
- Williams, T., 2001. Intermittent swimming by mammals: a strategy for increasing energetic efficiency during diving. *Am. Zool.* 41, 166–176. <https://doi.org/10.1093/icb/41.2.166>.
- Wu, G., Yang, Y., Zeng, L., 2007. Kinematics, hydrodynamics and energetic advantages of burst-and-coast swimming of koi carps (*Cyprinus carpio koi*). *J. Exp. Biol.* 210, 2181–2191. <https://doi.org/10.1242/jeb.001842>.
- Xia, D., Chen, W., Liu, J., Wu, Z., Cao, Y., 2015. The three-dimensional hydrodynamics of thunniform swimming under self-propulsion. *Ocean Eng.* 110, 1–14. <https://doi.org/10.1016/j.oceaneng.2015.10.008>.
- Xia, D., Chen, W., Liu, J., Luo, X., 2018. The energy-saving advantages of burst-and-glide mode for thunniform swimming. *J. Hydronaut.* 30, 1072–1082. <https://doi.org/10.1007/s42241-018-0120-8>.
- Xiao, Q., Liao, W., 2010. Numerical investigation of angle of attack profile on propulsion performance of an oscillating foil. *Comput. Fluids* 39, 1366–1380. <https://doi.org/10.1016/j.compfluid.2010.04.006>.
- Zhang, N., Zheng, Z.C., 2009. Flow/pressure characteristics for flow over two tandem swimming fish. *Comput. Fluids* 38, 1059–1064. <https://doi.org/10.1016/j.compfluid.2008.01.016>.
- Xu, G.D., Duan, W.Y., Xu, W.H., 2017. The propulsion of two flapping foils with tandem configuration and vortex interactions. *Phys. Fluids* 29 (97102). <https://doi.org/10.1063/1.5001501>.
- Zhang, Y., Kihara, H., Abe, K., 2018. Three-dimensional simulation of a self-propelled fish-like body swimming in a channel. *Eng. Appl. Comput. Fluid Mech.* 12, 473–492. <https://doi.org/10.1080/19942060.2018.1453381>.
- Zhu, Q., Wolfgang, M., Yue, D., Triantafyllou, M., 2002. Three-dimensional flow structures and vorticity control in fish-like swimming. *J. Fluid Mech.* 468, 1–28. <https://doi.org/10.1017/S002211200200143X>.